Published in final edited form as:
Nat Microbiol. 2017 December ; 2(12): 1635–1647. doi:10.1038/s41564-017-0038-x.

D-alanine esterification of teichoic acids contributes to *Lactobacillus plantarum* mediated *Drosophila* growth promotion upon chronic undernutrition

Renata C. Matos[1], **Martin Schwarzer**[1], **Hugo Gervais**[1], **Pascal Courtin**[2], **Pauline Joncour**[1], **Benjamin Gillet**[1], **Dali Ma**[1], **Anne-Laure Bulteau**[1], **Maria Elena Martino**[1], **Sandrine Hughes**[1], **Marie-Pierre Chapot-Chartier**[2], and **François Leulier**[1,*]

[1]Institut de Génomique Fonctionnelle de Lyon (IGFL), Université de Lyon, Ecole Normale Supérieure de Lyon, CNRS UMR 5242, Université Claude Bernard Lyon 1, 69364 Lyon Cedex 07, France

[2]Micalis Institute, INRA, AgroParisTech, Université Paris-Saclay, 78350 Jouy-en-Josas, France

Summary

The microbial environment influence animal physiology. However, the underlying molecular mechanisms of such functional interactions are largely undefined. Previously, we showed that upon chronic undernutrition, strains of *Lactobacillus plantarum,* a major commensal partner of *Drosophila*, promote host juvenile growth and maturation partly via enhanced expression of intestinal peptidases. By screening a transposon insertion library of *Lactobacillus plantarum* in gnotobiotic *Drosophila* larvae, we identify a bacterial cell wall modifying machinery encoded by the *pbpX2-dlt* operon that is critical to enhance host digestive capabilities and promote animal growth and maturation. Deletion of this operon leads to bacterial cell wall alteration with a complete loss of teichoic acids D-alanylation. We show that *L. plantarum* cell walls bearing D-alanylated teichoic acids are directly sensed by *Drosophila* enterocytes to ensure optimal intestinal peptidase expression and activity, juvenile growth and maturation upon chronic undernutrition. We thus conclude that besides peptidoglycan, teichoic acids modifications participate in the host-commensal bacteria molecular dialogue occurring in the intestine.

Keywords

Symbiosis; Microbiota; Commensal; Drosophila; Lactobacillus; Teichoic acids

*Correspondence: francois.leulier@ens-lyon.fr.

Author contributions

FL supervised the work. RCM and FL designed the experiments. RCM, MS, ALB, DM and HG performed the experiments. BG and SH designed and performed high-throughput insertion tracking by deep sequencing. MEM and PJ performed the insertions sites bioinformatics analysis. PC performed D-alanine and PG quantifications. ALB developed the protocol for proteolytic activity determination. RCM, ALB, PC, MPCC, MS, and FL analyzed the results. RCM and FL wrote the manuscript.

Data availability

The data that support the findings of this study are available from the corresponding author upon request.

Introduction

Metazoans establish complex interactions with their resident microorganisms for mutual benefits1–3. When in homeostasis, these interactions contribute to different aspects of host physiology3–5. In the gut, microbial communities enhance digestive efficiency by providing enzymatic functions that help their hosts optimize extraction of dietary energy and nutrients. In addition, the gut microbiota promotes proper immune system development, local immune homeostasis and limits pathogen colonization6–8. Despite the renewed interest in understanding the functional impact of gut microbiota on host physiology, a clear view of the molecular dialogue engaged upon host/microbiota interaction remains elusive9,10. Therefore the use of simple animal models, such as *Drosophila*, may help unravel the evolutionarily conserved mechanisms underlying the impact of intestinal bacteria in their host physiology, since it combines genetic and experimental tractability with a cultivable microbiota and the ease to generate germ-free animals11,12.

Drosophila gut microbiota is composed of simple and aerotolerant bacterial communities (mostly *Acetobacteraceae* and *Lactobacillaceae* families) with five prevalent species: *Acetobacter pomorum*, *Acetobacter tropicalis*, *Lactobacillus brevis*, *Lactobacillus plantarum* and *Lactobacillus fructivorans*13,14. The genus *Lactobacillus* gathers bacteria with high phylogenetic and functional diversity15,16. They have been largely used as model lactic acid bacteria and are recognized as potential health beneficial microorganisms in the human gastrointestinal tract17,18. As a prevalent member of *Drosophila* microbiota, *L. plantarum* is involved in several aspects of host physiology such as social behaviour11,19, protection against infection3,20, gut epithelial homeostasis21,22, nutrition23–25 and post-embryonic development3,4,23,26. We previously reported that, upon chronic undernutrition, certain strains of *L. plantarum* (such as *L. plantarum*^{WJL}, *Lp*^{WJL}) fully recapitulate the beneficial effect of a more complex microbiota by promoting *Drosophila* juvenile growth and maturation rate4,23. *Lp*^{WJL} exerts its beneficial effect on larval growth through the host nutrient sensing system that relies on the tissue specific activity of the TOR kinase, which subsequently modulates hormonal signals controlling growth and maturation4,27. Importantly, using conventional and gnotobiotic mice we recently demonstrated that the intestinal microbiota and some strains of *L. plantarum* also influence linear growth in mammals3,11. These results suggest that the still unknown molecular mechanisms underlying microbiota-mediated juvenile growth promotion are likely conserved during evolution. Recently, we showed that *L. plantarum* influences juvenile growth at least partly through the increased expression of a set of specific host digestive enzymes in the intestine1,3. We have shown that *Lp*^{WJL} promotes the expression of peptidases, such as Jon66Ci and Jon66Cii, in the enterocytes in both PGRP-LE/Imd/Relish-dependent and independent manner. The resulting enhanced peptidase activity in the midgut increases the digestion of dietary proteins into dipeptides and amino acids as well as their uptake. Circulating dipeptides and amino acids are sensed in endocrine tissues by the TOR kinase pathway, which promotes the production of *Drosophila* growth factors, the insulin-like peptides (dILPs) and a precocious pic of production of the molting steroid hormone Ecdysone3,4.

Here, we aim to identify the bacterial genetic determinants involved in *L. plantarum*-mediated juvenile growth promotion. Through the generation of a random transposon-mediated insertion library in the growth promoting strain *L. plantarum*^{NC8} (*Lp*^{NC8}), we identified a set of transposon insertions altering host growth promotion. Among these insertions, we further characterized the insertion in the *pbpX2-dlt* operon with predicted functions in cell wall biogenesis and remodelling. Deletion of this operon alters the bacterial cell wall due to complete loss of teichoic acids D-alanylation, and significantly impairs *Drosophila* larval growth, maturation and intestinal peptidases expression and activity. Our analysis points to the existence of additional host sensing and signalling mechanisms, besides PGRP-LE/Imd/Relish, involved in the sensing of the cell wall features defined by the gene products of *pbpX2-dlt* operon. Taken together our results demonstrate that D-alanine esterification of teichoic acids directly contributes to *L. plantarum* mediated *Drosophila* growth promotion upon chronic undernutrition.

Results

Generation of a *L. plantarum*^{NC8} random-mutagenesis library

To identify *L. plantarum* genes required to sustain *Drosophila* juvenile growth and maturation, we adopted a classical unbiased forward genetic approach via transposon-mediated mutagenesis of the bacterial chromosome coupled to a phenotypical screening in mono-colonized animals. The previously characterized strain *Lp*^{WJL} has low transformation efficiency (Matos R., unpublished results) and carries plasmids6,8,28,29 that preclude random transposition in the bacterial chromosome. We therefore chose a *L. plantarum* strain with high transformation efficiency, no native plasmids and capable to promote host growth in mono-association experiments to the same extent as *Lp*^{WJL}. This strain, designated as *Lp*^{NC8}, is suitable for transposon mutagenesis library construction3,9. Upon mono-colonization both strains strongly support *Drosophila*'s larval linear growth (Fig. 1a) and maturation (i.e entry to metamorphosis; Fig. 1b) under chronic undernutrition when compared to the moderate growth promoting strain *L. plantarum*^{NIZO2877} (*Lp*^{NIZO2877} 11,30 or the germ-free (GF) condition (Fig. 1a-b). Thus, we mutagenized the *Lp*^{NC8} chromosome using the P_{junc}-TpaseIS$_{1223}$ transposon mutagenesis system previously described by3,13. This system was developed for lactic acid bacteria and has been successfully applied to *Lactobacillus casei*3,15 and *Lactobacillus pentosus*9,17. It couples a thermo-sensitive plasmid (pVI129) expressing transiently the IS$_{1223}$ transposase and a suicide plasmid (pVI110) encoding the IS$_{1223}$ transposon, which together lead to random insertion of IS$_{1223}$ sequences into the bacterial chromosome. Strain NC8pVI129 (Supplementary Table 1) was transformed with pVI110 and 2091 colonies were randomly selected and stocked as individual clones at -80°C. To evaluate the randomness of the transposon insertions in our library, we tracked transposon insertion sites by deep sequencing of flanking genomic sequences (see Methods). Sequencing reads were mapped to the *Lp*^{NC8} genome, which revealed that transposon insertions are evenly distributed over *Lp*^{NC8} genome with an average insertion site every 2kb (Fig. 1c). By analysing sequencing reads and insertions sites, we found that among the 2091 insertions, 1574 insertions disrupted 1218 different ORFs (42% of *Lp*^{NC8} ORFs currently annotated; Supplementary Table 2) and 517 landed in intergenic regions. Insertions were detected in ORFs belonging to different clusters of

orthologous groups (COGs) (Supplementary Table 2; Supplementary Figure 1) and globally, only minimal differences in the relative proportion of functional groups targeted in our library were observed as compared to the repartition of COGs in the *Lp*^{NC8} genome (Supplementary Figure 1). These results demonstrate the insertion library sufficiently covers the genome in random manner, thus making it suitable for further phenotypic screen.

Screening of the *Lp*^{NC8} mutant library identifies mutants affecting larval growth promotion

We screened the insertions library with the aim to identify *Lp*^{NC8} mutants, which upon mono-colonization have an altered capacity to sustain growth and maturation of chronically undernourished *Drosophila*. Prior to the library screening, we experimentally determined that in these nutritional conditions, the most robust timing to visually discriminate (by counting the number of pupae emerging from food) a strong growth promoting strain (*Lp*^{NC8}), a moderate growth promoting strain (*Lp*^{NIZO2877} 11,13) and the GF condition is day 8 after GF eggs inoculation with bacterial isolates (Fig. 1b, Supplementary Figure 2). We searched for *Lp*$^{NC8\text{-}pVI110}$ insertion mutants with a growth promotion capacity weaker or similar to *Lp*^{NIZO2877} (Fig. 1b, Supplementary Figure 2). The screen was conducted as follow: 20 GF eggs were deposited in tubes containing low-yeast diet which were inoculated independently with each one of the 2091 *Lp*$^{NC8\text{-}pVI110}$ insertion strains, while *Lp*^{NIZO2877}, *Lp*^{NC8} and GF served as controls. After 8 days of development, the number of emerging pupae was scored in each tube and normalized into z scores (i.e the score for each strain reflecting the number of standard deviations from the mean number of pupae scored at day 8 from all tested strains; mean=15,18 pupae, SD=3,53; Fig. 1D). The control strains yielded z scores of -0,05 for *Lp*^{NC8} and -3,73 for *Lp*^{NIZO2877}. This screen revealed insertions leading to either gain or loss of function phenotypes as compared to the reference strain *Lp*^{NC8} with z scores ranging from +2,73 down to -4,52 (Fig. 1d). In order to select robust loss-of-function candidates similar or stronger than the *Lp*^{NIZO2877} strain, we set a selection cut-off for z scores below -3 and identified 28 transposon insertion mutants, which were retained for a secondary screening procedure. These candidates were re-tested in 3 independent experiments as during the primary screen but this time the number of emerging pupae was recorded at days 7, 8 and 9. From the secondary screen, we confirmed that 7 insertion mutants robustly delayed pupariation time with statistical significance when compared to the wild-type (WT) *Lp*^{NC8} strain and were statistically undistinguishable from the *Lp*^{NIZO2877} strain (Fig. 1e-f). To exclude the possibility that the loss of the growth promoting phenotype of these 7 mutants was a consequence of their inability to persist in the low yeast fly food, we assessed bacterial loads in the food matrix at days 3, 5, 7 and 10 after initial inoculation of 10^8 CFUs.mL^{-1} for each strain (Supplementary Figure 3). All the mutant strains behave as the *Lp*^{NC8} strain at each time point.

Having characterized the impact of the 7 insertion mutants on *Drosophila* growth promotion, we identified the transposon insertion sites in *Lp*^{NC8} genome. Of the 7 insertions, 6 were inside ORFs and 1 in an intergenic region between the ORFs encoding the transporter *secE* and the transcription regulator *nusG* (Table 1 and Supplementary Figure 4). The insertions in ORFs hit the *mleP1* gene encoding a malate transport protein (referred to as 1-74), the *pbpX2* gene encoding a putative serine-type D-D-carboxypeptidase (referred to as 6-20), the *pts28ABC* gene encoding a PTS system component (referred to as 14-10), the *lp_2466* gene

encoding a prophage terminase large subunit (referred to as 17-57), the *lp_1944* gene encoding an ABC transporter (referred to as 18-65) and the *dnaK* gene encoding a chaperone protein (referred to as 22-19) (Table 1). Previously, we reported that peptidoglycan (PG) recognition by PGRP-LE partly contributes to Lp^{WJL}-mediated intestinal peptidase enhanced expression during juvenile growth promotion 3,31. Hence, we were intrigued by the 6-20 mutant, hitting *pbpX2,* with a predicted function in PG biosynthesis/maturation21,23, we thus pursued the characterization of the 6-20 mutant.

Deletion of *pbpX2-dlt* operon affects Lp^{NC8} mediated larval growth promotion

To confirm the loss-of-function phenotype observed with the transposon insertion mutant 6-20, we generated a deletion mutant of the *pbpX2* gene in the Lp^{NC8} strain by homology-based recombination (Δ*pbpX2*; Fig. 2a). We tested the ability of the newly constructed Δ*pbpX2* strain to promote *Drosophila*'s growth by determining larval size seven days post-inoculation (Fig. 2b). We also assessed the developmental timing (Fig. 2c) of GF eggs monoassociated with either Δ*pbpX2* or the Lp^{NC8} (WT) strain. Larvae associated with Δ*pbpX2* strain are significantly smaller than those associated with Lp^{NC8} and their larval development is significantly delayed (Fig. 2b-d). These results confirm the importance of *pbpX2* gene to Lp^{NC8} growth promoting effect. However the effect observed in Δ*pbpX2* strain is not as pronounced as the one observed with the 6-20 insertion mutant (Fig. 2b-d). The *pbpX2* gene is located in the *dlt* locus and is the first ORF of an operon that encodes 5 additional genes located in 3' position to *pbpX2*, the *dlt* genes (*dltXABCD*; Fig. 2a; Palumbo et al., 2006). Given that *pbpX2* is co-transcribed with *dltXABCD* genes 23, we wondered if the 6-20 insertion in the Lp^{NC8} strain would generate a polar effect and disrupt the entire operon and not only the *pbpX2* gene. To test our hypothesis, we engineered two strains deleted for the entire *pbpX2-dlt* operon (Δdlt_{op}) or only for the *dlt* genes (Δdlt_{XABCD}) by homology-based recombination (Fig. 2a). We tested the Δdlt_{op} and Δdlt_{XABCD} mutants in larval size and developmental timing assays and observed that Δdlt_{XABCD} phenocopies Δ*pbpX2* and only Δdlt_{op} recapitulated the 6-20 mutant phenotype, showing an increased loss of function phenotype as compared to Δ*pbpX2* and Δdlt_{XABCD} mutants (Fig. 2b-d). Thus, we conclude that the 6-20 insertion in the Lp^{NC8} strain disrupts the entire *pbpX2-dlt* operon (and not just *pbpX2*) and that both *pbpX2* and the *dlt* genes encode important functionalities in Lp^{NC8} to promote *Drosophila*'s growth.

We next wondered if an altered colonization of the larvae by the mutant bacteria caused the Δdlt_{op} loss of function phenotype. To test this hypothesis we quantified the load of Lp^{NC8} and mutant bacteria associated to surface-sterilized and size-matched larvae. We did not detect a significant difference between the ability of Lp^{NC8} and Δdlt_{op} cells to associate with the larvae (Fig. 2e). This result indicates that the altered larval growth promotion of the Δdlt_{op} mutant is not caused by a general disruption of the association between *Drosophila* larvae and its symbiont but probably by a rupture of the molecular dialogue engaged between these symbiotic partners.

Deletion of *pbpX2-dlt* operon in Lp^{NC8} impacts cell morphology, D-alanylation of TA but not bacterial growth dynamics

Previously, inactivation of the operon encoding *dlt* genes in the strain *L. plantarum*^{WCFS1} (Lp^{WCFS1}) and the strain *Lactobacillus rhamnosus*^{GG} (Lr^{GG}) had been associated with a major reduction of esterification of lipoteichoic acids (LTA) by D-alanines, reduced bacterial growth rate and increased cell lysis21,23,26. Therefore we investigated Lp^{NC8} and Δdlt_{op} mutant growth dynamics by following optical density (at 600 nm) and CFU counts in liquid cultures (Supplementary Figure 5). Similarly to the *dltB* mutant in the Lp^{WCSF1} strain21,23 Δdlt_{op} mutant enters stationary phase with lower OD_{600} value. However, while studying CFU counts, we did not detect any significant differences in bacterial cells doubling time (Supplementary Figure 5; 98 minutes for Lp^{NC8} *vs* 94 minutes for Δdlt_{op}). This is in line with our previous results posing that the 6-20 mutant bacteria persist in the low-yeast fly food similarly to wild-type Lp^{NC8} cells (Supplementary Figure 3) and that Δdlt_{op} mutant cells colonize larvae like Lp^{NC8} cells (Fig. 2e). This striking difference between CFU counts and absorbance at 600nm for the two strains prompted us to study the cell morphology of Lp^{NC8} and Δdlt_{op} strains by phase contrast and fluorescence microscopy following membrane staining with FM4-64 (Fig. 3a). We detected a significant reduction of the width of Δdlt_{op} mutant cells (Fig. 3a; Lp^{NC8} mean width of 783 nm ±105; Δdlt_{op} mean width of 658 nm ±104). Scanning and transmission electron microscopy confirmed the reduced bacterial mid-cell width of Δdlt_{op} vs Lp^{NC8} cells (Fig. 3b-c). These observations are reminiscent of the *dlt* genes loss of function phenotypes seen in Lp^{WCFS1} and Lr^{GG}, yet, in contrast to those strains, the change in cell shape of $Lp^{NC8\text{-}\Delta dltop}$ mutant is not associated with reduced cell viability.

Next, we determined the amount of D-alanine esterified to teichoic acids of Lp^{NC8} and Δdlt_{op} strains. D-alanine was released from dried bacteria by mild alkaline hydrolysis and was quantified by HPLC (Fig. 3d-e) as described previously27,32, allowing to estimate D-alanine esterified to both lipoteichoic acids (LTA) and wall teichoic acids (WTA). D-alanine was released in appreciable amounts from Lp^{NC8} cells but was almost undetectable from the Δdlt_{op} cells (Fig. 3d-e). We therefore conclude that the deletion of *pbpX2-dlt* operon leads to a loss of D-alanine esterification on teichoic acids and width reduction in the mutant cells. Thus, these observations indicate that D-alanine esterification of teichoic acids (TA) is required for Lp^{NC8} mediated *Drosophila* growth promotion upon chronic undernutrition.

pbpX2-dlt dependant cell wall modification directly influence larval growth

Altering cell wall may have pleiotropic effects on bacterial cell physiology21. We therefore wondered if the identified *pbpX2-dlt* dependant cell wall modification influences larval growth directly (for example through direct host sensing and signaling of cell wall motifs) or indirectly (for example by indirectly altering the production of other functional compounds/metabolites by the mutant bacteria). To this end, we treated daily GF, Δdlt_{op} and Lp^{NC8} associated animals with cell walls purified from either Lp^{NC8} or Δdlt_{op} cells (Fig. 3f). We observed that none of the treatments with purified cell walls triggers enhanced growth of GF larvae. However, treatments with cell walls purified from Lp^{NC8} but not from Δdlt_{op} cells could rescue the altered growth of Δdlt_{op} associated animals while they did not influence growth of Lp^{NC8} associated animals. These results therefore establish that purified cell walls

on their own are not sufficient to trigger enhanced larval growth in GF animals but demonstrate that *pbpX2-dlt* dependant cell wall modification is necessary and sufficient to directly influence growth of *L. plantarum* associated animals.

Deletion of *pbpX2-dlt* operon impacts intestinal peptidase expression

We previously reported that upon chronic undernutrition, *L. plantarum* promotes *Drosophila* larval growth partly by increasing the expression and activity of a set of intestinal peptidases3,32. The activity of the PGRP-LE/Imd/Relish signalling cascade in the enterocytes regulates the expression of some intestinal peptidases in the presence of *L. plantarum*, but loss of function mutations in the PGRP-LE/Imd/Relish cascade only partially dampen peptidase induction upon mono-association3,33. We thus postulated that in addition to PG sensing by PGRP-LE followed by Imd/Relish signalling, additional compounds produced by the bacteria would impact intestinal peptidase expression and activity through yet unknown mechanisms. Given that Δdlt_{op} strain is a poor *Drosophila* growth promoting strain with an altered cell wall composition, we hypothesize that the *pbpX2-dlt* dependent D-alanine esterification of TA might be an additional bacterial signal sensed by enterocytes to trigger intestinal peptidase expression.

To test this hypothesis, we investigated how the Δdlt_{op} strain influences intestinal peptidases expression and activity. To this end, we inoculated GF eggs with either sterile PBS, Lp^{NC8} or Δdlt_{op} strains, collected size matched larvae at mid-L3 stage, dissected their midguts and assayed intestinal peptidase activity and expression (Fig. 4a). We detected increased peptidase activity in the midgut of Lp^{NC8} associated animals as compared to GF midguts and such induction was diminished in Δdlt_{op} associated animals (Fig. 4b). Accordingly, among the intestinal peptidase genes previously reported to be induced upon *L. plantarum* association3,23, two (*Jon66Cii* and *Jon65Ai*), show a significantly reduced induction in Δdlt_{op} associated animals as compared to Lp^{NC8} associated animals (Fig. 4c and Supplementary Figure 6a). Given the direct influence of *pbpX2-dlt* dependant cell wall modification on larvae growth, we tested if purified cell wall would trigger intestinal peptidase expression. To this end, we acutely treated GF animals at mid-L3 with cell wall purified from either Lp^{NC8} or Δdlt_{op} cells, and assayed intestinal peptidase genes expression in dissected midguts (Fig. 4d). At 6 hours post-inoculation cell walls purified from Lp^{NC8} induced *Jon66Cii* expression while cell walls purified from Δdlt_{op} cells did not. At 24 hours post-inoculation cell walls purified from Δdlt_{op} cells now triggered *Jon66Cii* increased expression albeit to a significantly reduced level than upon Lp^{NC8} cell walls treatment. Of note, we noticed that *Jon66Cii* and *Jon65Ai* genes induction upon acute treatment purified cell wall or live cells did not fully recapitulate the extent of gene induction observed upon chronic treatment with live cells (Supplementary Figure 6), however the host transcriptional response to acute treatment with purified cell wall is very similar to the response to acute treatment with live cells (Supplementary Figure 6d). Taken collectively these results establish that *Drosophila* enterocytes directly sense cell walls bearing *pbpX2-dlt* dependent D-alanine esterification of TA, a signal that selectively triggers intestinal peptidase induction.

Europe PMC Funders Author Manuscripts

Sensing of multiple cell wall motifs is required for Lp^{NC8} mediated intestinal peptidase expression and larval growth promotion

Next, we tested if the impaired induction of intestinal peptidases by Δ*dlt*$_{op}$ cells and purified cell wall is further altered in *Dredd* larvae. *Dredd* encodes an essential positive regulator of the PG-sensing Imd/Relish cascade26,28,29. In *Dredd* larvae, the PGRP-LE/Imd/Relish signalling cascade is completely inactivated in the enterocytes upon *L. plantarum* association3,34,35. We confirmed this observation by analysing the expression of several Imd/Relish target genes (*PGRP-SC1*, *attD*, *PGRP-LB* and *Pirk*30,36) whose expression in the midgut entirely relies on the PGRP-LE/Imd/Relish cascade upon *L. plantarum* association3,23,26. We found that while *PGRP-SC1, attD*, *PGRP-LB* and *Pirk* failed to be induced by either cells or purified cell wall from Lp^{NC8} or Δ*dlt*$_{op}$ mutant in *Dredd* larvae, both bacterial strains and purified cell walls readily activated their expression in control larvae with no difference between the two bacterial strains (Supplementary Figure 6b-c). These results therefore indicate that the Δ*dlt*$_{op}$ deletion does not alter the Dredd-dependent sensing of *L.plantarum* PG by the wild-type host. This result suggests that the effect mediated through *L. plantarum* cell walls bearing D-alanylated TA activates another commensal-sensing and signalling pathway in enterocytes in addition to the PGRP-LE/Imd/Relish cascade, which probably directly senses D-alanylated TA.

Next, we wished to examine if this second commensal sensing host pathway genetically interacts with the Dredd-dependent PG sensing pathway, and how such interaction affects expression of intestinal peptidases in response to *L. plantarum*. We therefore analysed the expression of the intestinal peptidases in dissected midguts from *Dredd* larvae monoassociated with either Lp^{NC8} or Δ*dlt*$_{op}$ cells (Fig. 4c and Supplementary Figure 6a) or acutely inoculated with their purified cell walls (Fig. 4d-e). In contrast to control larvae, where only *Jon66Cii* and *Jon65Ai* expression were altered, the expression of *Jon66Cii*, *Jon65Ai*, *Jon66Ci, CG18179, CG18180, Jon99Ci* and *Jon44E* peptidases in *Dredd* mutants was strongly altered upon Δ*dlt*$_{op}$ strain association or its purified cell walls inoculation as compared to the Lp^{NC8} condition.

This result, combined with our expression study of the PGRP-LE/Imd/Relish targets (Supplementary Figure 6b-c), illustrates that the mechanisms sensing cell walls bearing D-alanylated TA act in concert with Dredd-dependent PG sensing to elicit optimal expression response from intestinal peptidases loci. In the presence of Δ*dlt*$_{op}$ mutation, the host mechanisms sensing cell walls bearing D-alanylated TA is impaired, and the *Dredd* mutation exacerbates the Δ*dlt*$_{op}$-related host response, which culminates to diminish intestinal peptidase expression. Since the Δ*dlt*$_{op}$ mutation abolishes the D-alanine esterification of bacterial TA, our results indicate that the host enterocytes sense and signal the presence of *L. plantarum* cells by at least two mechanisms, (1) through PGRP-LE-mediated PG fragment recognition and Imd/Relish signalling and (2) sensing of D-alanylated TA and signalling by yet to discover host mechanisms (Fig. 5d).

Sensing of multiple cell wall motifs is required for Lp^{NC8} mediated larval growth promotion

Finally, we probed the consequence on *L. plantarum* mediated larval growth promotion of altering both bacterial signals. We previously showed that altering Dredd-dependent PG

sensing in the enterocytes was not sufficient to alter *L. plantarum*-mediated *Drosophila* growth promotion 3,37–39. Here we compared the larval growth and maturation of control and *Dredd* animals upon association with either the Lp^{NC8} or Δdlt_{op} strains. We observed a significant effect on both larval growth (Fig. 5a) and maturation (Fig. 5b-c) of coupling the Δdlt_{op} bacterial genotype and the host *Dredd* genotype. Taken together these results demonstrate that the host machineries sensing and signalling bacterial PG and cell walls bearing D-alanylated TA, in enterocytes are required for optimal *L. plantarum* mediated *Drosophila* growth and maturation upon chronic undernutrition (Fig. 5d).

Discussion

The results obtained in this study identify the *L. plantarum pbpX2-dlt* operon as encoding an important bacterial functionality required to sustain a host-commensal dialogue that is beneficial to the host. Deletion of *pbpX2-dltXABCD* genes results in impairment of *L. plantarum* mediated *Drosophila* gut peptidases expression and activity, larval growth and maturation. We show that the *pbpX2-dlt* operon is a key genetic determinant shaping *L. plantarum* cell wall and cell shape via D-alanine esterification of TAs. Moreover, we reveal that these changes in the cell envelope architecture and composition are critical for bacterial cell wall sensing and signaling by *Drosophila* enterocytes, which underlies the beneficial interaction between *Drosophila* and its symbiont *L. plantarum* leading to improved growth upon chronic undernutrition.

Despite *L. plantarum* being model lactic acid bacteria, random transposon mutagenesis is difficult to achieve due to low-transformation efficiencies and/or instability of the transposon-delivering vector3,9. Here, we successfully employed the P_{junc}-$TpaseIS_{1223}$ system13,29 by constructing a random transposon mutant library in Lp^{NC8}. We collected and screened 2091 transposon insertion mutants covering 1218 genes and tested around 42% of the predicted protein coding sequences in the Lp^{NC8} genome3,31. By increasing the number of transposon insertion mutants one could target virtually all non-essential genes. Upon screening of our library for its ability to promote larval growth after association with each one of the insertion mutants, we identified 7 insertions that severely impaired *L. plantarum* growth promotion phenotype. Though significantly different from Lp^{NC8}, none of the insertions reflects a complete loss-of-function phenotype that completely mimics the GF condition. This observation suggests that *L. plantarum* growth promotion effect is probably multifactorial and to achieve such a "GF-like" phenotype we would need to target multiple bacterial functions.

Among the 7 insertions, we were particularly interested by the one impacting the *pbpX2-dlt* operon, which is involved in *L. plantarum* cell wall biogenesis and remodelling, and whose deletion impaired significantly *Drosophila* larval growth and interfered with host peptidase expression. Cell wall structure, composition and organization play major roles in host-bacteria dialogue as they represent the core bacteria components that trigger the initial microbe sensing response in the host. *pbpX2* encodes a putative D-D-carboxypeptidase with homology to various low-molecular weight penicillin binding proteins11,23. The presence of *pbpX2* upstream of the *dlt* genes is a unique feature of *L. plantarum* genomes3,23, but the physiological role of *pbpX2* and the importance of the genetic linkage between *pbpX2* and

the *dlt* genes remain unknown. The *dlt* genes are well described in several gram-positive bacteria as being responsible for the esterification of teichoic acids with D-alanine34,39–41. Teichoic acids (TA) are anionic polymers localized within the gram-positive bacteria cell wall, representing up to 50% of the cell envelope dry weight3,21,28. There are two types of TA: wall teichoic acids (WTA), which are covalently bound to PG, and lipoteichoic acids (LTA), which are anchored on the cytoplasmic membrane13,21. The current model states that initially DltA ligates D-alanine onto the carrier protein DltC. With the help of DltB, D-alanine is then transferred from DltC to undecaprenyl phosphate crossing the membrane, where DltD transfers the D-alanine to LTA32. Although still not fully understood, it seems that D-alanyl-LTA serves as donor for D-alanine substitutions in WTA32. Despite being encoded upstream of *dltA* in several gram-positive bacteria, the role of DltX in TA D-alanylation remains unknown. Lp^{NC8} carries in its genome the genetic information to produce both types of TA33. Attachment of D-alanine substituents to these structures is an important mechanism by which bacteria modulates surface charge, whose level has a major impact on TAs functionalities, such as the control of autolysis23, maintenance of cell wall morphology26 and signalling with cells of their animal host34,36,41. *L. plantarum* strains lacking D-alanine substitutions on their TAs reduce secretion of proinflammatory cytokines but better stimulate IL-10 production in peripheral blood monocytes when compared to its WT, showing the importance of TA D-alanylation in immunomodulating properties in mammals34,35. To our knowledge, direct sensing of TA and downstream signalling events have never been reported in *Drosophila,* yet D-alanylation of WTA seems an important bacterial feature impacting immunomodulation since its hampers recognition of *Staphylococcus aureus* PG by the pattern recognition receptor PGRP-SA36.

By quantification of D-alanine released from whole cells we determined that *pbpX2-dlt* operon is responsible for D-alanylation of TA in Lp^{NC8}. Moreover, the absence of the *pbpX2-dlt* operon impacts cell morphology in Lp^{NC8} while cell viability or growth dynamics are not affected in contrast to other lactobacilli strains23,26. The consequences of deleting *dlt* genes in lactobacilli are therefore strain dependent. This study highlights the role of *pbpX2-dltXABCD* genes and their impact on TA D-alanine esterification for a bacterial beneficial effect on its host, a feature that is traditionally associated with pathogenesis and antibiotic resistance of gram-positive bacteria37–39. Our results strengthen the role of TA modifications on commensal-host interactions and pave the way to further studies aiming at pinpointing the effect of *pbpX2-dlt* function on *L. plantarum* cell biology and physiology as well as probing the physiological role of *pbpX2*.

We previously established that the promotion of *Drosophila* linear growth by *L. plantarum* is partly dependent on increased expression of host peptidases. We also demonstrated that such increased peptidases expression is partly controlled by PGRP-LE/Imd/Relish signalling cascade3, a signalling pathway triggered by DAP containing PG fragments29. Here we show that *pbpX2-dlt* dependent modification of bacterial cell walls also contributes to host intestinal peptidase induction and *Drosophila* larval growth in parallel to PG sensing. In this study, we observed in WT hosts a reduced peptidases expression and activity upon association with the Δdlt_{op} strain when compared to the WT *L. plantarum* strain. This differential peptidases expression is exacerbated in animals impaired in Imd/Relish signalling. Specifically, in *Dredd* mutants, peptidases expression upon Δdlt_{op} strain

association or Δ*dlt*$_{op}$ purified cell walls treatment is close to the GF condition. Moreover, low peptidases expression upon Δ*dlt*$_{op}$ in *Dredd* mutants correlates to poor larval growth and maturation. Previously, we have established that the promotion of larval growth and maturation by *L. plantarum* requires optimal expression of intestinal peptidases partially through PG-dependent Imd signalling. Imd deficient individuals have impaired PG sensing; yet in this context *L. plantarum* still significantly promotes peptidases induction and larval growth3. This observation indicates that *L. plantarum* must be detected by additional sensing mechanisms beyond PG recognition. In the current study, we show that the absence of *pbpX2-dltXABCD* genes in *Lp*^{NC8} depletes D-alanine from TA and that cell walls deprived of D-alanylated TA lack the additional bacterial signal sensed by *Drosophila* enterocytes to trigger intestinal peptidases induction and systemic growth. Our results therefore indicate that bacterial cell walls bearing D-alanylated TA are directly sensed by *Drosophila* enterocytes through a dual mechanism: (1) PGRP-LE-mediated PG fragment recognition and Imd/Relish signalling and (2) direct sensing of D-alanylated TA and signalling by yet to discover host mechanisms (Fig. 5d).

Previously, we established that promotion of intestinal peptidase expression and activity upon *L. plantarum* association was necessary and sufficient to sustain host systemic growth3, however it is clear that the intestinal peptidase response does not account for the entire host growth promotion conferred by *L. plantarum.* Our new study revealing a dual *L. plantarum* sensing strategy by the host now paves the way to identify the full complement of the intestinal responses engaged upon such sensing events and required beside intestinal peptidases induction to ensure optimal growth promotion. Our study also reveals that even if *L. plantarum* sensing strategies are genetically altered (such as in *Dredd* mutant associated with Δ*dlt*$_{op}$), *L. plantarum* retains a residual but significant host growth promotion capabilities, which to date remains elusive and will be the focus of future investigations.

Taken collectively, our study unravels a central molecular dialogue engaged between chronically undernourished *Drosophila* and its commensal partner *L. plantarum*, which supports the beneficial nature of their symbiosis. Given the recent demonstration of the conservation of the beneficial effects of *L. plantarum* on the linear growth of chronically undernourished gnotobiotic mouse models11, our results therefore pave the way to probing whether this molecular dialogue is conserved in mammals.

Materials and Methods

Drosophila diets, stocks and breeding

Drosophila stocks were cultured as described in3. Briefly, flies were kept at 25°C with 12/12 hours dark/light cycles on a yeast/cornmeal medium containing 50 g/L of inactivated yeast. The poor yeast diet was obtained by reducing the amount of inactivated yeast to 6 g/L. Germ-free stocks were established as described in1. Axenicity was routinely tested by plating serial dilutions of animal lysates on nutrient agar plates. *Drosophila y,*w flies were used as the reference strain in this work. The following *Drosophila* line was also used: *y,w,Dredd*^{F64} 3,28.

Bacterial strains and growth conditions

Strains used in this study are listed in Supplementary Table 1. *E. coli* strains were grown at 37°C in LB medium with agitation. *L. plantarum* strains were grown in static conditions in MRS media at 37°C, unless differently stated. Erythromycin antibiotic was used at 5 μg/mL for *L. plantarum* and 150 μg/mL for *E. coli*.

Random transposon mutagenesis of *L. plantarum*^{NC8}

L. plantarum mutagenesis was performed using the P_{junc}-TpaseIS$_{1223}$ system as previously described by13 and17. Briefly, electrocompetent *L. plantarum*^{NC8} cells were first transformed with pVI129, resulting in the NC8pVI129 strain. Electrocompetent cells of NC8pVI129 strain were transformed with pVI110, plated on MRS plates supplemented with 5 μg/mL of erythromycin and incubated for 48 h at 42°C to select for integrants. 2091 tn-insertion mutants were individually stored at -80°C.

Library high throughput insertion tracking: library construction and deep sequencing

Genomic DNA was extracted from each transposon insertion mutant by pools of 96 (UltraClean Microbial DNA isolation kit, MoBio). 22 DNA pools were quantified using Qubit system 2.0 (Invitrogen) and mixed together in equimolar proportion (4 μg / pool). DNA was sheared (1μg) following the manufacturer instructions using the S220 focused ultrasonicator (Covaris) to obtain a fragment distribution length from 100 bp to 1 kb, with an average peak around 400 bp. All the fragmented DNA material was then used to build a library using the Ion Xpress Plus gDNA Fragment Library Preparation kit (Thermofisher) following the protocol of the kit. However, only the P1 adapter was ligated at this step and not both adapters, A and P1, as usual. We designed a biotinylated fusion primer (named Primer Fusion A-IRL hereafter) containing: the sequence of the A adapter, the IRL sequence (transposon-specific primer IRL described in 42) and a biotin at the 5' end (reference Biot-TEG, Eurogentec) (Supplementary Table 3). A PCR amplification was performed using the P1 primer and the primer fusion A-IRL, and the ligated-P1 DNA as a template. Reagents in the PCR mix were as follow: 1 μl of each primer at 10 μM, 47 μl of Platinum PCR SuperMix High Fidelity (Thermofisher), 1 μl of DNA at 50ng/μl for a final volume of 50 μl. After a denaturation step of 5 min at 95°C, 20 cycles of amplification were performed (15 s at 95°C; 15 s at 58°C; 1 min at 70°C), followed by a final extension step of 5 min at 70°C. The aim of this amplification step is to target the IRL sequence in the P1-library fragments, and add simultaneously the A adapter to build the final library, both A and P1 adapters being necessary for the subsequent sequencing. The fragments in the good configuration (meaning containing the biotinylated primer) were selected using Streptavidin magnetic beads (Dynabeads MyOne Streptavidin C1, Invitrogen) according to the manufacturer instructions. The biotinylated-selected amplicons were then purified using Qiagen MiniElute kit in order to eliminate the sodium hydroxyde, and re-amplified for 5 cycles following the classical re-amplification library protocol described in the Ion Xpress Plus gDNA Fragment Library Preparation kit (Thermofisher). The library was then size-selected using the E-gel Electrophoresis system (Invitrogen) in order to select fragments from 350 to 450 bp in length. The library was qualified according to the concentration and distribution profile using the TapeStation 2200 (Agilent). The diluted library (6 pM) was amplified through

Europe PMC Funders Author Manuscripts

emulsion PCR using the Ion PGM Template OT2 400 kit (Thermofisher). Finally, the enriched library was loaded into a 314v2 chip and sequenced on the Ion PGM sequencer with the Ion PGM HiQ chemistry.

Library high throughput insertion tracking by deep sequencing: bio-informatics analysis

A dedicated R script has been created to obtain mapping information of the reads on Lp^{NC8} genome. The script takes in input the alignment sam file of the reads on the reference genome and compares the positions of the reads with an annotation table of the Lp^{NC8} genome obtained with Geneious from the Lp^{NC8} PubMed genbank file. It returns a table saying for each read if it maps a gene partially or totally or if it maps an intergenic region.

BLAST Ring Image Generator (BRIG)

Visual analysis of the distribution of the transposon insertions was done by using BRIG43; http://sourceforge.net/projects/brig/). Lp^{NC8} was used as the reference genome. BRIG uses CGView44 to render maps and is operated using a graphical user interface. The BRIG method uses the software BLASTALL v 2.2.25+ for the searches. The analysis was done with default settings.

Library screening for loss of growth promotion phenotype

The screen was performed in the poor yeast diet. Each transposon insertion mutant ($1x10^8$ CFUs) was used to independently inoculate 20 *y,w* germ-free eggs and incubated at 25°C for 8 days. The number of pupae 8 days after egg laying was scored for each of the 2091 tn-insertion mutants. Those values were converted in z-scores (where μ=15,18 n=2091 and σ =3,53).

Sequence analysis and mapping of transposon insertion site

pVI110 locus of insertion were confirmed for the 8 loss-of-function mutant as described by17, with the following modifications. Genomic DNA was digested sequentially with ClaI and BstBI restriction enzymes (NEB). Digested fragments were ligated using T4 DNA ligase (NEB) accordingly to manufacture's instructions. Products of ligation were transformed into *E. coli* TG1 thermo-competent cells, in which circularized fragments containing the transposon behave as plasmids. Plasmids were isolated and sequenced (Genewiz) with the primers OLB221 and OLB215 (Supplementary Table 3). Identification of transposon target sequences was performed with the BLAST software from the National Center for Biotechnology Information (NCBI).

Construction of Δ*pbpX2*, Δ*dltXABCD* and Δdlt_{op} deleted strains in *L. plantarum*^{NC8} using pG+host9

Independent markerless deletions on *pbpX2* (Δ*pbpX2*), *dltX* to *dltD* (Δ*dltXABCD*) and *pbpX2* to *dltD* (Δdlt_{op}) genes were constructed through homology-based recombination with double-crossing over. Briefly, the 5′- and 3′-terminal regions of each region were PCR-amplified with Q5 High-Fidelity 2X Master Mix (NEB) from *L. plantarum* NC8 chromosomal DNA. Primers contained overlapping regions with pG+host945 to allow for Gibson Assembly. PCR amplifications were made using the following primers: OL118/

OL119 and OL120/OL121 (*pbpX2*), OL195/OL196 and OL197 and OL198 (*dltXABCD*), OL144/OL145 and OL146/OL147 (dlt_{op}) listed in Supplementary Table 3. The resulting plasmids (Supplementary Table 1) obtained by Gibson Assembly (NEB) were transformed into NC8 electrocompetent cells and selected at the permissive temperature (28°C) on MRS plates supplemented with 5 μg/mL of erythromycin. Overnight cultures grown under the same conditions were diluted and shifted to the non-permissive temperature (42°C) in the presence of 5 μg/mL of erythromycin to select single crossover integrants. Plasmid excision by a second recombination event was promoted by growing integrants at the permissive temperature without erythromycin. Deletions were confirmed by PCR followed by sequencing with primers OL126/OL127 (*pbpX2*), OL126/OL149 (*dltXABCD*) and OL148/OL149 (dlt_{op}).

Quantification of D-alanine from teichoic acids by high-performance liquid chromatography (HPLC)

D-alanine esterified to teichoic acids was detected and quantified as described by27. Briefly, D-alanine was released from whole heat-inactivated bacteria by mild alkaline hydrolysis with 0.1 N NaOH for 1h at 37°C. After neutralization, the extract was incubated with Marfey's reagent (1-fluoro-2,4-dinitrophenyl-5-L-alanine amide; Sigma). This reagent reacts with the optical isomers of amino acids to form diastereomeric *N*-aryl derivatives, which can be separated by HPLC. Separation of the amino acid derivatives was performed on a C_{18} reversed-phase column (Zorbax Eclipse Plus C18 RRHD 2.1x50mm 1.8μm Agilent) with an Agilent UHPLC 1290 system with a linear elution gradient of acetonitrile in 20 mM sodium acetate buffer (pH 4) as described previously 27. The eluted compounds were detected by UV absorbance at 340 nm. Quantification was achieved by comparison with D-alanine standards in the range of 100 to 1500 pmol. Mean values were obtained from five independent cultures with two injections for each.

Purification of *L. plantarum* cell wall

L. plantarum cells were grown in MRS medium and harvest at mid-exponential phase. After being washed with MilliQ water, cells were boiled for 10 min and centrifuged at 5000g at 4°C. $3.75x10^{10}$ CFUs were resuspended in 1 mL of SDS 5% in 50 mM of MES (Sigma-M8250) pH 5.5, pre-heated at 60°C and boiled for 25 min. After centrifugation at 20000g, pellets were resuspended in 1 mL of SDS SDS 5% in 50 mM of MES pH 5.5, pre-heated at 60°C and boiled for 15 min and then washed with MilliQ water to remove SDS traces. Next, pellets were sequentially enzymatically treated with 2 mg/mL of pronase (Roche 165921) in 50 mM of MES (Sigma-M8250) pH 6.0 for 90 min at 60°C; 200 μg/mL of trypsin (Sigma T-0303) in 50 mM of MES (Sigma-M8250) pH 6.0 for 2 h at 37°C under shaking; DNase (Sigma-D-4527) and RNase (Sigma-R-5503) (50 μg/mL) in 50 mM of MES (Sigma-M8250) pH 6.0 for 1 h at 37°C. After boiling for 15 min with SDS 2% in 50 mM of MES (Sigma-M8250) pH 5.5 and centrifuged at 20000g for 10 min, pellets were washed with MilliQ water to remove SDS traces. Purified cell walls (containing PG, WTA and polysaccharides) were finally lyophilized until use and for mass determination. We have confirmed that D-alanine esterification was kept on WTA in the purified cell walls of wild-type Lp^{NC8} whereas it was absent in the Δdlt_{op} mutant cell walls, using the protocol described above

Purified cell wall quantification

Purified cell walls were quantified by measuring muramic acid content in peptidoglycan after acid hydrolysis. Purified cell walls (200 µg) were hydrolyzed by 6 N HCl for 16 h at 100 °C under vacuum. Samples were then dried under vacuum and resuspended in 100 µl MilliQ H2O. Muramic acid (Mur) was quantified by high performance anion exchange chromatography coupled with pulse amperometric detection (HPAEC-PAD) as described previously by46, with an ICS5000 system (Thermo Scientific). Samples (20 µl) were injected on a Dionex CarboPac PA-1 anion exchange column (4 x 250 mm) (Thermo Scientific) with a guard column and eluted at a flow rate of 1 ml/min and a temperature of 30°C. Three eluents were used consisting of: MilliQ H_2O (eluent A), 150 mM NaOH (eluent B) and 150 mM sodium acetate in 100 mM NaOH (eluent C). The separation of Mur from other cell wall sugars and aminoacids was achieved by a first isocratic step of 20 % eluent B for 10 min followed by a linear gradient (0-100 %) of eluent C over 40 min, and finally with 100 % eluent C for 5 min. PAD detection operated with a gold working electrode and an Ag/AgCl combination reference electrode (Thermo scientific). Quantification was made with a standard curve of pure Mur (Sigma-Aldrich) (50 to 1000 pmol). The amount of PG in purified cell walls from Lp^{NC8} and Δdlt_{op} cells was determined to 151 nmol/mg and 162 nmol/mg, respectively.

Larval size measurements

Axenic adults were put overnight in breeding cages to lay eggs on sterile poor yeast diet. Fresh axenic embryos were collected the next morning and seeded by pools of 40 on 55 mm petri dishes containing fly food. $1x10^8$ CFUs (unless otherwise specified) or PBS were then inoculated homogenously on the substrate and the eggs. Petri dishes are incubated at 25°C until larvae collection. *Drosophila* larvae, 7 days after inoculation (unless otherwise specified), were randomly collected and processed as described by3. Individual larval longitudinal length of individual larvae was quantified using ImageJ software47. For the cell wall experiments supplementation, 170 nmol of purified cell wall (resuspended in PBS; corresponding to the amount of cell wall extracted from 10^8 CFUs) were added to the fly food every day until day 6.

Developmental timing determination

Axenic adults were put overnight in breeding cages to lay eggs on sterile poor yeast diet. Fresh axenic embryos were collected the next morning and seeded by pools of 40 in tubes containing fly food. $1x10^8$ CFUs of each strain (unless otherwise specified) or PBS were then inoculated homogenously on the substrate and the eggs and incubated at 25°C. Pupae emergence was scored every day until all pupae have emerged. D50 was determined using D50App (http://paulinejoncour.shinyapps.io/D50App) which is a Shiny app that calculates for the pupae emerged during a developmental experiment, the day when fifty percent of the pupae emerged. It takes as input a table with the number of pupae emerged every day for each condition and calculates with a local linear regression the day when fifty percent of the pupae emerged.

Bacterial loads analysis

For larval loads, *y,w* axenic eggs were inoculated with $1x10^8$ CFU of each strain and incubated at 25°C until collection. Larvae were harvested from the nutritive substrate and surface-sterilized with a 30 s bath in 70% EtOH under agitation and rinsed in sterile water. Pools of five larvae were deposited in 1.5 mL microtubes containing 0,75-1 mm glass microbeads and 500 μL of PBS. To access bacterial CFU in the fly nutritional matrix, microtubes containing food were inoculated with $1x10^7$ CFUs of each strain, independently. Tubes were incubated at 25°C until being processed. For bacterial load quantification, 0.75-1 mm glass microbeads and 500 μL PBS was added directly into the microtubes. Samples were homogenized with the Precellys 24 tissue homogenizer (Bertin Technologies). Lysates dilutions (in PBS) were plated on MRS agar using the Easyspiral automatic plater (Intersciences). MRS agar plates were then incubated for 24 h at 37°C. Bacterial concentration was deduced from CFU counts on MRS agar plates using the automatic colony counter Scan1200 (Intersciences) and its counting software.

Phase contrast and fluorescent imaging

Microscopy was performed on exponentially growing cells (OD600 = 0.3). Bacterial cultures (10 ml) were washed in PBS, centrifuged (3000g, 10 min) and resuspended in 150 mL of PBS. Bacterial cells were stained with FM4-64 (TermoFisher Scientific) at final concentration 0.1 mg/ml and incubated 5 min at room temperature in the dark. Slides were visualized with a Zeiss AxioObserver Z1 microscope fitted with an Orca-R2 C10600 charge-coupled device (CCD) camera (Hamamatsu) with a 100× NA 1.46 objective. Images were collected with axiovision (Carl Zeiss) and cell width at the half of the cell length (mid-width) was determined on phase contrast images by ImageJ using the MicrobeJ plug-in 48.

Scanning electron microscopy

Bacterial suspensions immersed in a fixative solution (2,5% glutaraldehyde in 0.2 M sodium cacodylate buffer, pH 7.4) were deposited on sterile cover-glasses discs (Marienfeld, VWR, France) and stored 1 hour at room temperature and overnight at 4°C. The fixative was removed, and samples were rinsed three times for 10 min in the sodium cacodylate solution (pH 7.4). The samples underwent progressive dehydration by soaking in a graded series of ethanol (50 to 100%) before critical point drying under CO_2. Samples were mounted on aluminum stubs (10 mm diameter) with carbon adhesive discs (Agar Scientific, Oxford Instruments SAS, GOMETZ-LA-VILLE, France) and sputter coated with gold-palladium (Polaron SC7640, Elexience, Verrières-le-buisson, France) for 200 s at 10 mA. Samples were then visualized by field emission gun scanning electron microscopy. They were viewed as secondary electron images (2 kV) with a Hitachi S4500 instrument (Elexience, Verrières-le-buisson, France). Scanning Electron Microscopy analyses were performed at the Microscopy and Imaging Platform MIMA2 (INRA, Jouy-en-Josas, France). Cell width at the half of the cell length (mid-width) was determined by ImageJ using the MicrobeJ plug-in48.

Transmission electron microscopy

Pellets of bacteria were fixed with 2% glutaraldehyde in 0.1 M Na cacodylate buffer pH 7.2, for 1 hour at room temperature. Samples were then contrasted with Oolong Tea Extract (OTE) 0.5% in cacodylate buffer, postfixed with 1% osmium tetroxide containing 1.5% potassium cyanoferrate, gradually dehydrated in ethanol (30% to 100%) and substituted gradually in mix of ethanol-epon and embedded in Epon (Delta microscopie – Labège France). Thin sections (70 nm) were collected onto 200 mesh cooper grids, and counterstained with lead citrate. Grids were examined with Hitachi HT7700 electron microscope operated at 80kV (Elexience – France), and images were acquired with a charge-coupled device camera (AMT). Transmission Electron Microscopy analyses were performed at the Microscopy and Imaging Platform MIMA2 (INRA, Jouy-en-Josas, France). Cell width at the half of the cell length (mid-width) was determined by ImageJ using the MicrobeJ plug-in48.

Intestinal peptidases activity

Five biological replicates of five midguts per condition were dissected in 100 µl of PBS and homogenized using a dounce homogenizer. The homogenate was then centrifuged at 10,000 ×*g* for 30 min at 4 °C. The 10,000×*g* supernatant represents the crude luminal and cytosolic fraction. Protein determinations were made using the BCA method (Pierce), with bovine serum albumin as a standard. Chymotrypsin activity of the peptidase was assayed using the fluorogenic peptide Ala-Ala-Phe-7-amido-4-methylcoumarin (25 µM). Assay was carried out using 10 µg of cytosolic protein in a total volume of 200 µl. The assay buffer was composed of 25 mM Tris-HCl at pH 7.5 and contained the appropriate peptide substrate. Enzymatic kinetics was conducted in a temperature-controlled microplate fluorimetric reader (Fluostar Galaxy, bMG, Stuttgart, Germany). Activity was measured by the release of L-aminomethyl-coumarin fluorescence over time (350/440 nm excitation/emission wavelengths). Activity is expressed as quantity of fluorescence emission per minute per µgram of proteins.

RNA extraction and RT-qPCR analysis

Axenic *y,w* and *y,w,Dredd* eggs were inoculated with $1x10^8$ CFU of Lp^{NC8} and Δdlt_{op} strains independently or kept axenic. Larvae were size matched for the three conditions and harvested at mid-L3 larval stage. Alternatively, larvae were kept axenic until mid-L3 stage and were inoculated with 170 nmol of purified cell wall from Lp^{NC8} and Δdlt_{op} for 6 and 24 hours. RNA extraction of five replicates of six dissected guts for each condition was performed as described by3. RT-qPCR was performed using gene-specific primer sets (Supplementary Table 3) as described by3. Results are presented as the value of $\Delta Ct^{gene}/\Delta Ct^{rp49}$.

Statistical analysis

Data representation and analysis was performed using Graphpad PRISM 6 software (www.graphpad.com). A total of 3 to 5 biological replicates were used for all experiments performed in this study in order to ensure representativity and statistical significance. All samples were included in the analysis. Experiments were done without blinding. Two-sided

Europe PMC Funders Author Manuscripts

Mann Whitney's test was applied to perform pairwise statistical analyses between conditions. Kruskal Wallis test was applied to perform statistical analyses between multiple (n>2) conditions followed by Dunn's test that corrects for multiple comparisons.

Supplementary Material

Refer to Web version on PubMed Central for supplementary material.

Acknowledgments

The authors would like to thank Maura Strigini and Gilles Storelli for critical reading and editing of the manuscript; Christophe Grangeasse for helpful discussions and help with bacterial cells imaging; Christina Login and Thierry Meylheuc from MIMA2 platform at INRA Jouy-en-Josas research center for TEM and SEM sample preparation and observation, respectively; the Arthro-Tools and PLATIM platforms of the SFR Biosciences (UMS3444/US8) for providing *Drosophila* and imaging facilities; the IGFL sequencing platform for deep sequencing; Pascale Serror for pG+host9 and Hélène Licandro-Seraut for P_{junc}-TpaseIS*1223* system. RCM thanks the "Fondation pour la Recherche Médicale" for financial support through a postdoctoral scholarship SPF20140129318. MEM was funded by the European Union's Horizon 2020 research and innovation programme under the Marie Sklodowska-Curie grant agreement N8659510. This work was funded by an ERC starting grant (FP7/2007-2013-N°309704). FL lab is supported by the FINOVI foundation and the EMBO Young Investigator Program. The authors declare no conflict of interests.

References

1. Erkosar B, et al. *Drosophila* Microbiota Modulates Host Metabolic Gene Expression via IMD/NF-κB Signaling. PLoS ONE. 2014; 9:e94729. [PubMed: 24733183]
2. Hooper LV, Gordon JI. Commensal host-bacterial relationships in the gut. Science. 2001; 292:1115–1118. [PubMed: 11352068]
3. Erkosar B, et al. Pathogen Virulence Impedes Mutualist-Mediated Enhancement of Host Juvenile Growth via Inhibition of Protein Digestion. Cell Host and Microbe. 2015; 18:445–455. [PubMed: 26439865]
4. Storelli G, et al. *Lactobacillus plantarum* Promotes *Drosophila* Systemic Growth by Modulating Hormonal Signals through TOR-Dependent Nutrient Sensing. Cell Metabolism. 2011; 14:403–414. [PubMed: 21907145]
5. McFall-Ngai M, et al. Animals in a bacterial world, a new imperative for the life sciences. Proceedings of the National Academy of Sciences. 2013; 110:3229–3236.
6. Kim E-K, Park YM, Lee OY, Lee W-J. Draft Genome Sequence of *Lactobacillus plantarum* Strain WJL, a Drosophila Gut Symbiont. Genome Announc. 2013; 1
7. Fraune S, Bosch TCG. Why bacteria matter in animal development and evolution. Bioessays. 2010; 32:571–580. [PubMed: 20544735]
8. Martino ME, et al. Resequencing of the *Lactobacillus plantarum* Strain WJL Genome. Genome Announc. 2015; 3
9. Gury JRM, Barthelmebs L, Cavin J-FO. Random transposon mutagenesis of *Lactobacillus plantarum* by using the pGh9:ISS1 vector to clone genes involved in the regulation of phenolic acid metabolism. Arch Microbiol. 2004; 182:337–345. [PubMed: 15375644]
10. Schroeder BO, Bäckhed F. Signals from the gut microbiota to distant organs in physiology and disease. Nat Med. 2016; 22:1079–1089. [PubMed: 27711063]
11. Schwarzer M, et al. *Lactobacillus plantarum* strain maintains growth of infant mice during chronic undernutrition. Science. 2016; 351:854–857. [PubMed: 26912894]
12. Ma D, Storelli G, Mitchell M, Leulier F. Studying host-microbiota mutualism in *Drosophila*: Harnessing the power of gnotobiotic flies. Biomed J. 2015; 38:285–293. [PubMed: 26068125]
13. Licandro-Seraut H, et al. Development of an Efficient In Vivo System (Pjunc-TpaseIS1223) for Random Transposon Mutagenesis of *Lactobacillus casei*. Applied and Environmental Microbiology. 2012; 78:5417–5423. [PubMed: 22610425]

Europe PMC Funders Author Manuscripts

14. Wong CNA, Ng P, Douglas AE. Low-diversity bacterial community in the gut of the fruitfly *Drosophila melanogaster*. Environmental Microbiology. 2011; 13:1889–1900. [PubMed: 21631690]
15. Licandro-Seraut H, Scornec H, Pedron T, Cavin JF, Sansonetti PJ. Functional genomics of *Lactobacillus casei* establishment in the gut. Proceedings of the National Academy of Sciences. 2014; doi: 10.1073/pnas.1411883111
16. Goh YJ, Klaenhammer TR. Genomic features of *Lactobacillus* species. Front Biosci (Landmark Ed). 2009; 14:1362–1386. [PubMed: 19273135]
17. Perpetuini G, et al. Identification of Critical Genes for Growth in Olive Brine by Transposon Mutagenesis of *Lactobacillus pentosus* C11. Applied and Environmental Microbiology. 2013; 79:4568–4575. [PubMed: 23686273]
18. Kleerebezem M, et al. The extracellular biology of the lactobacilli. FEMS Microbiol Rev. 2010; 34:199–230. [PubMed: 20088967]
19. Sharon G, et al. Commensal bacteria play a role in mating preference of *Drosophila melanogaster*. Proceedings of the National Academy of Sciences. 2010; 107:20051–20056.
20. Blum JE, Fischer CN, Miles J, Handelsman J. Frequent Replenishment Sustains the Beneficial Microbiome of *Drosophila melanogaster*. mBio. 2013; 4 e00860–13–e00860–13.
21. Neuhaus FC, Baddiley J. A Continuum of Anionic Charge: Structures and Functions of D-Alanyl-Teichoic Acids in Gram-Positive Bacteria. Microbiology and Molecular Biology Reviews. 2003; 67:686–723. [PubMed: 14665680]
22. Jones RM, et al. Symbiotic lactobacilli stimulate gut epithelial proliferation via Nox-mediated generation of reactive oxygen species. The EMBO Journal. 2013; 32:3017–3028. [PubMed: 24141879]
23. Palumbo E, et al. D-Alanyl Ester Depletion of Teichoic Acids in *Lactobacillus plantarum* Results in a Major Modification of Lipoteichoic Acid Composition and Cell Wall Perforations at the Septum Mediated by the Acm2 Autolysin. Journal of Bacteriology. 2006; 188:3709–3715. [PubMed: 16672624]
24. Newell PD, Douglas AE. Among-species interactions determine the impact of gut microbiota on nutrient allocation in *Drosophila melanogaster*. Applied and Environmental Microbiology. 2013; doi: 10.1128/AEM.02742-13
25. Wong ACN, Dobson AJ, Douglas AE. Gut microbiota dictates the metabolic response of *Drosophila* to diet. Journal of Experimental Biology. 2014; doi: 10.1242/jeb.101725
26. Perea Vélez M, et al. Functional analysis of D-alanylation of lipoteichoic acid in the probiotic strain *Lactobacillus rhamnosus* GG. Applied and Environmental Microbiology. 2007; 73:3595–3604. [PubMed: 17434999]
27. Kovács M, et al. A functional dlt operon, encoding proteins required for incorporation of d-alanine in teichoic acids in gram-positive bacteria, confers resistance to cationic antimicrobial peptides in *Streptococcus pneumoniae*. Journal of Bacteriology. 2006; 188:5797–5805. [PubMed: 16885447]
28. Leulier F, Rodriguez A, Khush RS, Abrams JM, Lemaitre B. The *Drosophila* caspase Dredd is required to resist gram-negative bacterial infection. EMBO Rep. 2000; 1:353–358. [PubMed: 11269502]
29. Leulier F, et al. The *Drosophila* immune system detects bacteria through specific peptidoglycan recognition. Nat Immunol. 2003; 4:478–484. [PubMed: 12692550]
30. Lhocine N, et al. PIMS Modulates Immune Tolerance by Negatively Regulating *Drosophila* Innate Immune Signaling. Cell Host and Microbe. 2008; 4:147–158. [PubMed: 18692774]
31. Axelsson L, et al. Genome Sequence of the Naturally Plasmid-Free *Lactobacillus plantarum* Strain NC8 (CCUG 61730). Journal of Bacteriology. 2012; 194:2391–2392. [PubMed: 22493200]
32. Reichmann NT, Cassona CP, Grundling A. Revised mechanism of D-alanine incorporation into cell wall polymers in Gram-positive bacteria. Microbiology. 2013; 159:1868–1877. [PubMed: 23858088]
33. Martino ME, et al. Nomadic lifestyle of *Lactobacillus plantarum* revealed by comparative genomics of 54 strains isolated from different habitats. Environmental Microbiology. 2016; doi: 10.1111/1462-2920.13455

34. Grangette C, et al. Enhanced antiinflammatory capacity of a Lactobacillus plantarum mutant synthesizing modified teichoic acids. Proc Natl Acad Sci USA. 2005; 102:10321–10326. [PubMed: 15985548]
35. Rigaux P, et al. Immunomodulatory properties of *Lactobacillus plantarum* and its use as a recombinant vaccine against mite allergy. Allergy. 2009; 64:406–414. [PubMed: 19120072]
36. Tabuchi Y, et al. Inhibitory Role for D-Alanylation of Wall Teichoic Acid in Activation of Insect Toll Pathway by Peptidoglycan of *Staphylococcus aureus*. The Journal of Immunology. 2010; 185:2424–2431. [PubMed: 20639481]
37. Kristian SA, et al. Alanylation of teichoic acids protects *Staphylococcus aureus* against Toll-like receptor 2-dependent host defense in a mouse tissue cage infection model. J Infect Dis. 2003; 188:414–423. [PubMed: 12870123]
38. Kristian SA, et al. D-alanylation of teichoic acids promotes group a streptococcus antimicrobial peptide resistance, neutrophil survival, and epithelial cell invasion. Journal of Bacteriology. 2005; 187:6719–6725. [PubMed: 16166534]
39. Peschel A, Vuong C, Otto M, Götz F. The D-alanine residues of *Staphylococcus aureus* teichoic acids alter the susceptibility to vancomycin and the activity of autolytic enzymes. Antimicrobial Agents and Chemotherapy. 2000; 44:2845–2847. [PubMed: 10991869]
40. Perego M, et al. Incorporation of D-alanine into lipoteichoic acid and wall teichoic acid in *Bacillus subtilis*. Identification of genes and regulation. J Biol Chem. 1995; 270:15598–15606. [PubMed: 7797557]
41. Smelt MJ, et al. The impact of *Lactobacillus plantarum* WCFS1 teichoic acid D-alanylation on the generation of effector and regulatory T-cells in healthy mice. PLoS ONE. 2013; 8:e63099. [PubMed: 23646181]
42. Scornec H, et al. Rapid 96-well plates DNA extraction and sequencing procedures to identify genome-wide transposon insertion sites in a difficult to lyse bacterium: *Lactobacillus casei*. Journal of Microbiological Methods. 2014; 106:1–5. [PubMed: 25091187]
43. Alikhan N-F, et al. BLAST Ring Image Generator (BRIG): simple prokaryote genome comparisons. BMC Genomics. 2011; 12:402. [PubMed: 21824423]
44. Stothard P, Wishart DS. Circular genome visualization and exploration using CGView. Bioinformatics. 2005; 21:537–539. [PubMed: 15479716]
45. Maguin E, et al. Efficient insertional mutagenesis in lactococci and other gram-positive bacteria. Journal of Bacteriology. 1996; 178:931–935. [PubMed: 8550537]
46. Clarke AJ. Compositional analysis of peptidoglycan by high-performance anion-exchange chromatography. Analytical Biochemistry. 1993; 212:344–350. [PubMed: 8214575]
47. Schneider CA, et al. NIH Image to ImageJ: 25 years of image analysis. Nature Methods. 2012; 9:671–675. [PubMed: 22930834]
48. Ducret A, et al. MicrobeJ, a tool for high throughput bacterial cell detection and quantitative analysis. Nat Microbiol. 2016; 1:16077. [PubMed: 27572972]

Europe PMC Funders Author Manuscripts

Europe PMC Funders Author Manuscripts

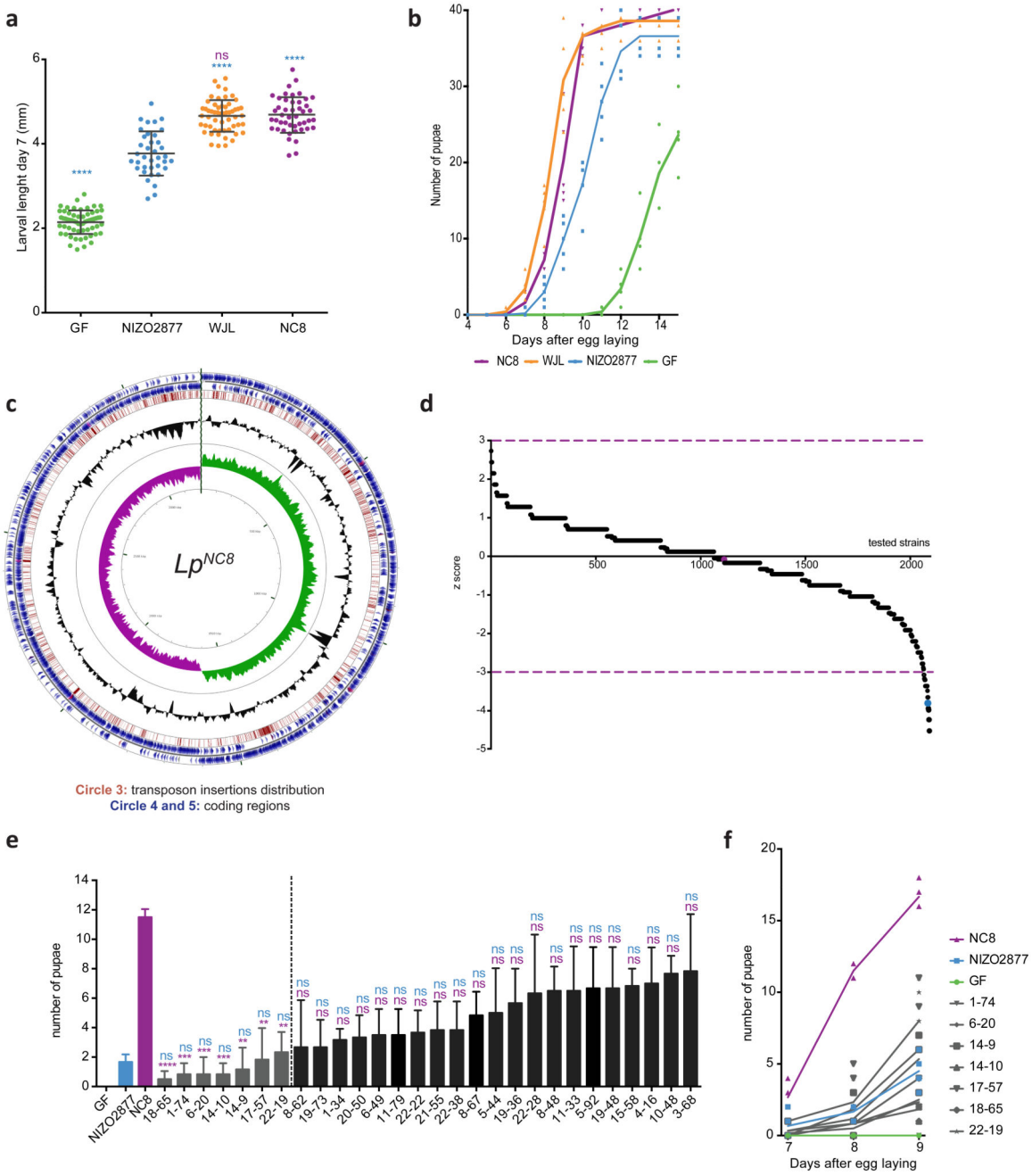

Figure 1. Identification of *L. plantarum*^{NC8} loci involved in *Drosophila* growth promotion.

(a) Larval longitudinal length after inoculation with Lp^{WJL} (n=56), Lp^{NC8} (n=60) and $Lp^{NIZO2877}$ (n=37) strains and PBS (n=60) for the GF condition. Larvae were collected 7 days after association and measured as described in the Methods section. Blue asterisks illustrate statistically significant difference with larval size of $Lp^{NIZO2877}$; *ns* represent absence of statistically significant difference between Lp^{WJL} and Lp^{NC8} larval sizes. ****: p<0,0001. Center values in the graph represent means and error bars represent SD. Representative graph from one out of three independent experiments. (b) Number of

emerged pupae scored over time from eggs associated with the strains Lp^{WJL}, Lp^{NC8}, $Lp^{NIZO2877}$ or PBS (for the GF condition). Forty GF eggs were associated independently with 10^8 CFUs of each one of the strains in 5 replicates. The number of pupae was scored every 24 h. (c) Genome atlas of transposon insertions mapped to Lp^{NC8} genome. The innermost rings represent the GC skew (Circle 1) in purple/green and GC content (Circle 2) in black. Circle 3 shows the distribution of the genomic regions disrupted by each transposon insertion (red bars). Circle 4 and 5 show Lp^{NC8} coding regions (blue arrows), tRNAs (red arrows) and rRNAs (purple arrows) on the negative and positive strand respectively. (d) Screen of the random transposon insertion library for mutants with altered growth promotion phenotype under chronic under-nutrition. The number of pupae scored at day 8 after association with the 2091 insertional mutants were converted in z-scores. Each strain was tested once. Purple lines indicate the cut off of z=+/-3. Control strains are represented by colored dots: Lp^{NC8} in purple and $Lp^{NIZO2877}$ in blue. (e) Number of emerged pupae 8 days after association of GF eggs with the 28 insertions selected form the primary screen after setting the z score at -3. Each strain was tested in 5 replicates. Center values in the graph represent means and error bars represent SD. Representative graph from one out of three independent experiments. Purple asterisks illustrate statistically significant difference with Lp^{NC8} number of pupae; *ns* represent absence of statistically significant difference with Lp^{NC8} (purple) and $Lp^{NIZO2877}$ (blue). ****: p<0,0001; ***: 0,0001<p<0,001; **: 0,001<p<0,01. The insertions on the left of the dotted line were retained for further analyses. (f) Number of emerged pupae at days 7, 8 and 9 after association of 20 GF eggs with 10^8 CFUs of the 7 insertions selected from the secondary screen. Each strain was tested in 5 replicates. Representative graph from one out of three independent experiments. For exact *p* values see Supplementary Table 4.

Europe PMC Funders Author Manuscripts

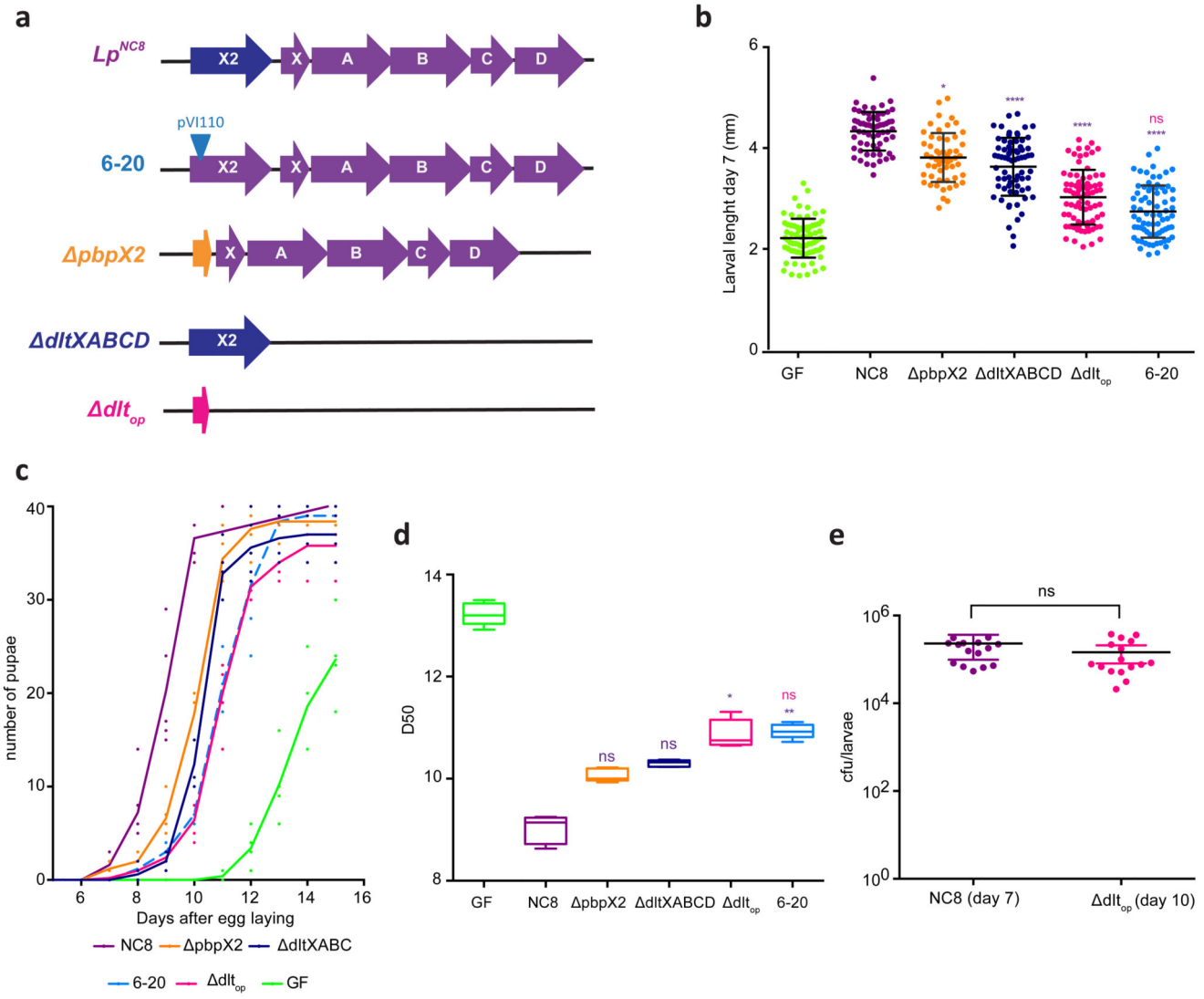

Figure 2. The *pbpX2-dlt* operon impacts *Drosophila*'s growth.

(a) *pbpX2-dlt* operon genomic organization in the Lp^{NC8} strain: *pbpX2/dltX/dltA/dltB/dltC/dltD*. 6-20, pVI110 insertion within *pbpX2* gene. Δ*pbpX2* mutant, in which *pbpX2* gene was deleted by homology-based recombination. Δ*dltXABCD* mutant, in which *dltXABCD* genes were deleted by homology-based recombination. Δdlt_{op} mutant, with genes *pbpX2/dltX/dltA/dltB/dltC/dltD* deleted by homology-based recombination. (b) Larval longitudinal length after inoculation with strains Lp^{NC8} (n=62), 6-20 (n=76), Δ*pbpX2* (n=55), Δ*dltXABCD* (n=70), Δdlt_{op} (n=76) or PBS (n= 73) (for the GF condition). Larvae were collected 7 days after association and measured as described in the Methods section. Purple asterisks illustrate statistically significant difference with Lp^{NC8} larval size; *ns* represent absence of statistically significant difference with Δdlt_{op}. ****: p<0,0001. Center values in the graph represent means and error bars represent SD. Representative graph from one out of three independent experiments. (c) Number of emerged pupae scored over time for eggs associated with strains Lp^{NC8}, 6-20, Δ*pbpX2,* Δ*dltXABCD,* Δdlt_{op} or PBS (for the GF

condition). Forty germ-free eggs were associated independently with 10^8 CFUs of each one of the strains in 5 replicates. The number of pupae was scored every 24h. Representative graph from one out of three independent experiments. (d) Day when fifty percent of pupae emerge during a developmental experiment (D50) for GF eggs associated with strains Lp^{NC8}, 6-20, Δ*pbpX2,* Δ*dltXABCD,* Δdlt_{op} or PBS (for the GF condition). Center values in the graph represent means. Purple asterisks illustrate statistically significant difference with Lp^{NC8} larval size; *ns* represent absence of statistically significant difference with Δdlt_{op}. ***: 0,0001<p<0,001; **: 0,001<p<0,01; *: p<0,05. (e) Bacterial load of size matched larvae associated with 10^8 CFUs of Lp^{NC8} (larvae collected 7 days after association) (n=16) or Δdlt_{op} (n=16) (larvae collected 10 days after association). Center values in the graph represent means and error bars represent SD. *ns* represents absence of statistically significant difference between the two conditions. The values refer to 4 independent experiments. For exact *p* values see Supplementary Table 4.

Europe PMC Funders Author Manuscripts

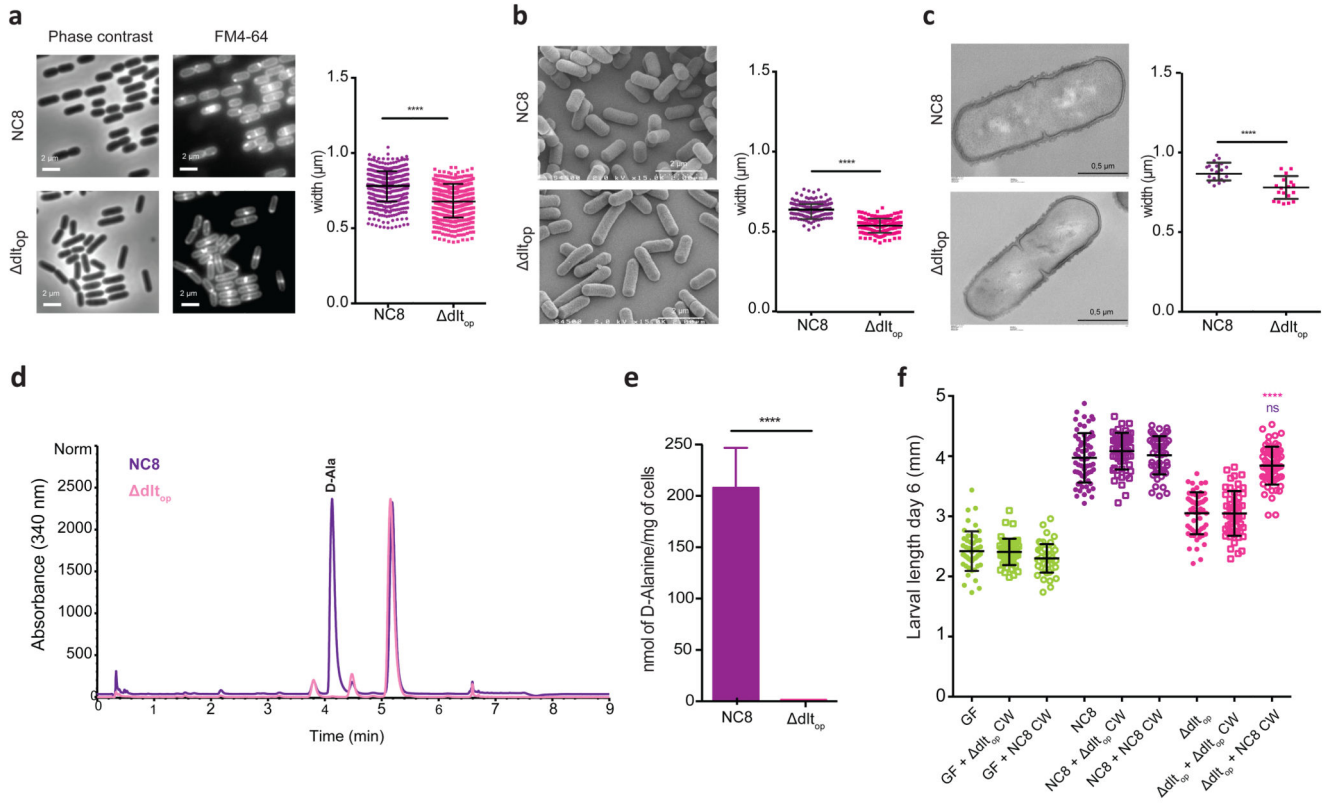

Figure 3. Cell envelope changes related to *pbpX2-dlt* operon deletion.

(a) Observation of Lp^{NC8} (n=489) and Δdlt_{op} (n=542) cells by phase contrast microscopy following membrane staining with FM4-64. Representative images from one out of three independent experiments. (b). Observation of Lp^{NC8} (n=159) and Δdlt_{op} (n=153) cells by scanning electron microscopy. (c). Observation of Lp^{NC8} (n=20) and Δdlt_{op} (n=21) cells by transmission electron microscopy. (a-c right panels) Lp^{NC8} and Δdlt_{op} cell width measurements from each microscopy observations. Center values in the graph represent means and error bars represent SD. (d) HPLC detection of D-alanine released from whole cells. D-alanine released by alkaline hydrolysis from Lp^{NC8} and Δdlt_{op} whole cells were derivatized with Marfey's reagent and separated by HPLC. D-alanine derivatives eluted at a retention time of 4.2 minutes. The eluted compounds were detected by UV absorbance at 340 nm. Quantification was achieved by comparison with D-alanine standards in the range of 100 to 1500 pmol. (e) Amount of D-alanine released from whole cells of Lp^{NC8} and Δdlt_{op} by alkaline hydrolysis and quantified by HPLC. Mean values were obtained from five independent cultures with two injections for each. (f) Larval longitudinal length after inoculation with strains Lp^{NC8} (n=62), Δdlt_{op} (n=58), PBS (n=50) and purified cell walls from Lp^{NC8} (GF + NC8 CW: n=51; NC8 + NC8 CW: n=51; NC8 + Δdlt_{op} CW: n=57) and Δdlt_{op} (GF + Δdlt_{op} CW: n=51; Δdlt_{op} + NC8 CW: n=64; Δdlt_{op} + Δdlt_{op} CW: n=55). Larvae were collected 6 days after the fist association and measured as described in the Methods section. Pink asterisks illustrate statistically significant difference with Δdlt_{op} larval size; *ns* represent absence of statistically significant difference with Lp^{NC8}. ****: p<0,0001. Center

Europe PMC Funders Author Manuscripts

values in the graph represent means and error bars represent SD. Representative graph from one out of three independent experiments. For exact *p* values see Supplementary Table 4.

Europe PMC Funders Author Manuscripts

Europe PMC Funders Author Manuscripts

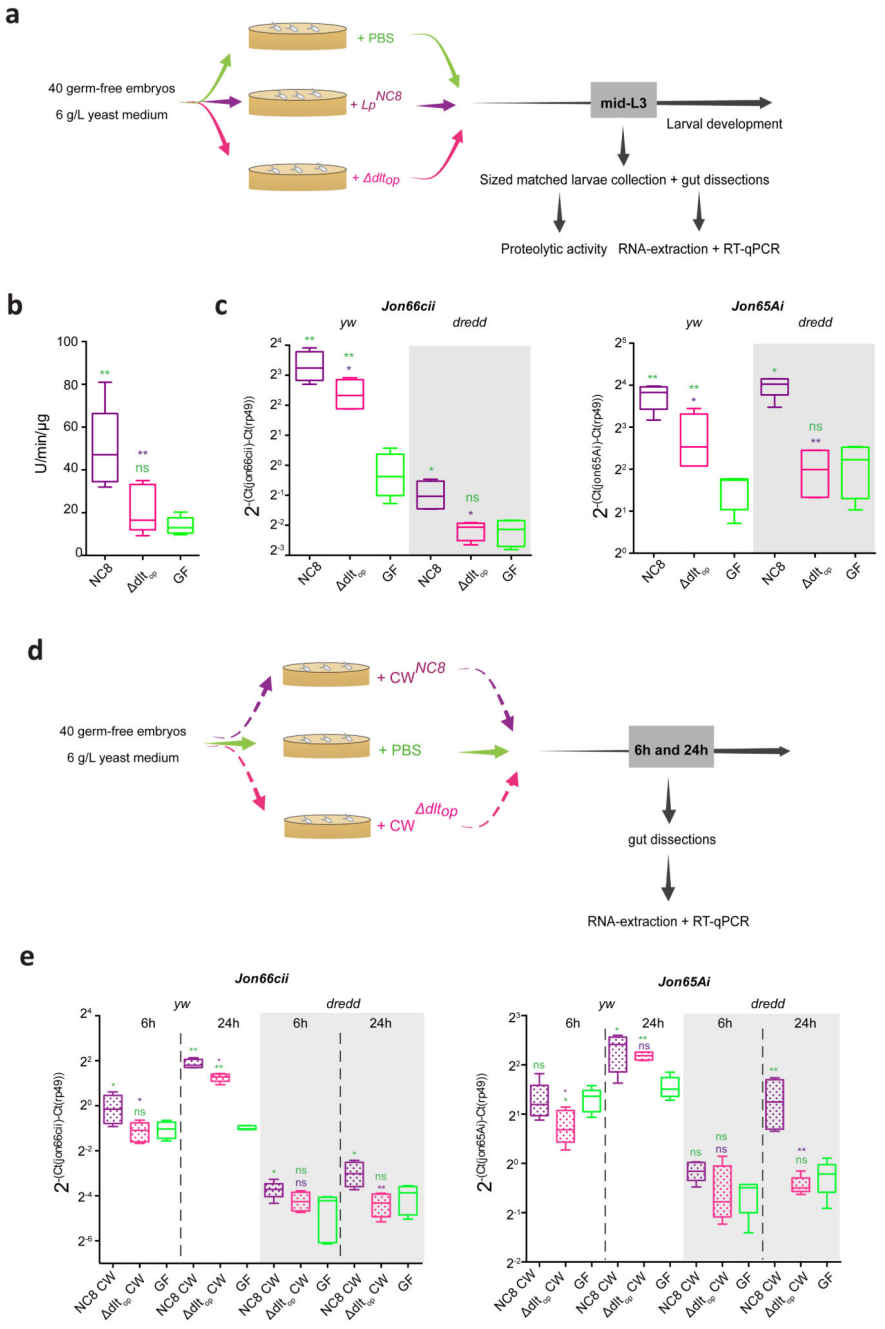

Figure 4. *Drosophila* reduced proteases expression in presence of Δ*dlt*$_{op}$ strain is independent of Imd pathway.

(a) Experimental set-up for proteolytic activity assessment and RT-qPCR analysis. Forty germ-free eggs of *y,w* and *y,w,Dredd* flies were inoculated with 10^8 CFUs of *Lp*^{NC8} or Δ*dlt*$_{op}$ strains. For each condition, size-matched larvae were collected at mid-L3 phases and their guts were dissected for proteolytic activity determination and RNA extraction followed by RT-qPCR. (b) Proteolytic activity of dissected guts associated with *Lp*^{NC8} or Δ*dlt*$_{op}$ strains. Center values in the graph represent means. Representative graph from one out of three independent experiments. Purple asterisks illustrate statistically significant difference

with Lp^{NC8} proteolytic activity. Green asterisks illustrate statistically significant difference with GF guts proteolytic activity. *ns* represent absence of statistically significant difference with GF guts proteolytic activity. **: 0,001<p<0,01. (c) Mean ± SD of $\Delta Ct^{gene}/\Delta Ct^{rp49}$ ratios for *Jon66Cii* and *Jon65Ai* detected in dissected guts associated with Lp^{NC8}, Δdlt_{op} or the GF condition from 5 biological replicates. Representative graphs from one out of three independent experiments. Purple asterisks illustrate statistically significant difference with Lp^{NC8} protease expression. Green asterisks illustrate statistically significant difference with GF condition. *ns* represent absence of statistically significant difference with GF condition. **: 0,001<p<0,01; *: p<0,05. (d) Experimental set-up to assess the direct sensing of bacterial cell wall (CW) by larvae. Forty germ-free eggs of *y,w* and *y,w,Dredd* flies were kept axenic until they reach mid-L3 stage (10 days after GF egg collection) upon which they were inoculated with purified cell walls from Lp^{NC8} or Δdlt_{op} strains. For each condition, larvae were collected at 6 or 24 hours after association and their guts were dissected for RNA extraction followed by RT-qPCR. (E) Mean ± SD of $\Delta Ct^{gene}/\Delta Ct^{rp49}$ ratios for *Jon66Cii* and *Jon65Ai* detected in guts of axenic larvae inoculated with purified cell walls from Lp^{NC8} and Δdlt_{op} or the GF condition from 5 biological replicates. Center values in the graph represent means. Representative graphs from one out of three independent experiments. Purple asterisks illustrate statistically significant difference with Lp^{NC8} protease expression. Green asterisks illustrate statistically significant difference with GF condition. Green *ns* represent absence of statistically significant difference with GF condition and purple with Lp^{NC8}. **: 0,001<p<0,01; *: p<0,05. For exact *p* values see Supplementary Table 4.

Europe PMC Funders Author Manuscripts

Europe PMC Funders Author Manuscripts

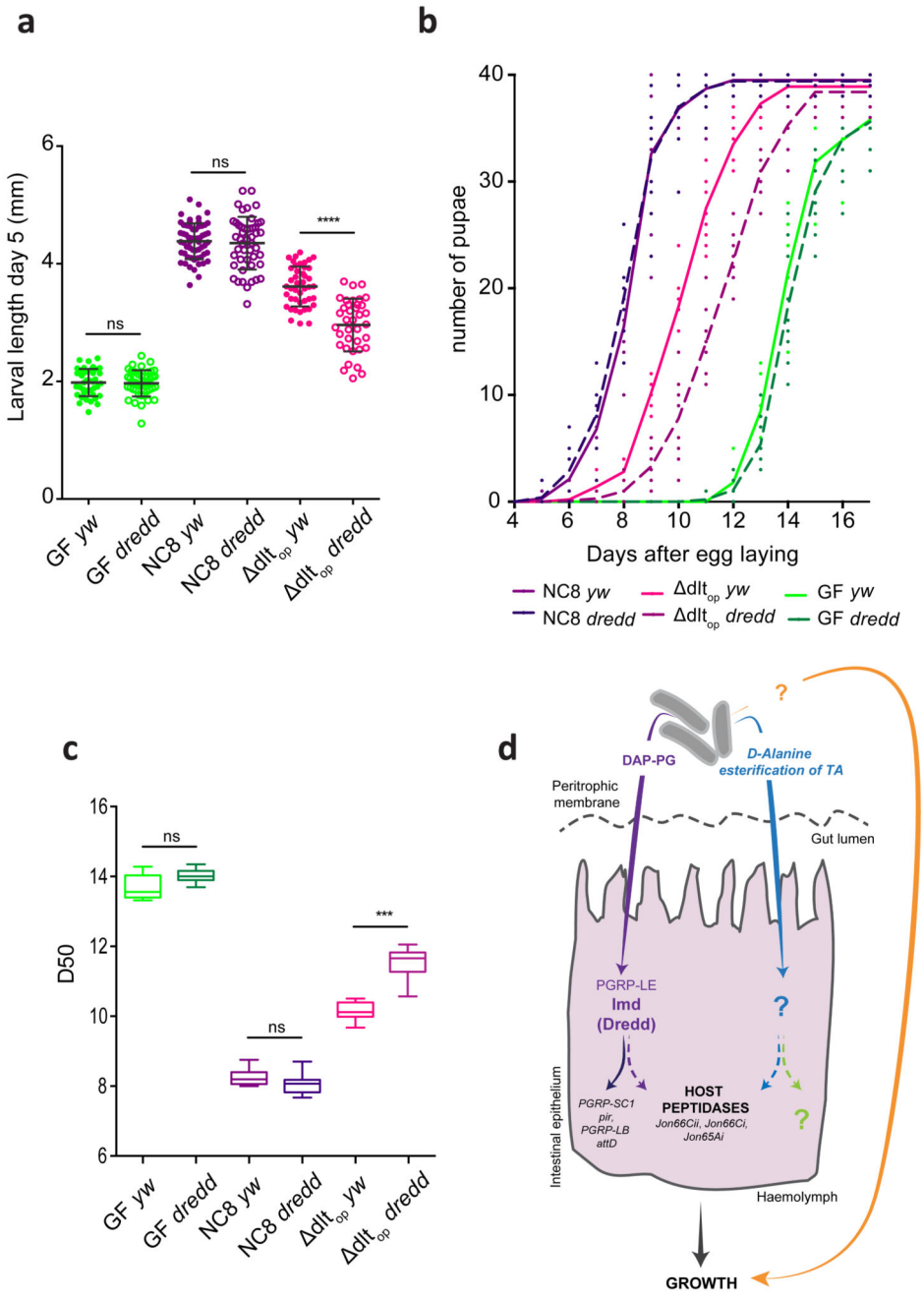

Figure 5. Sensing of multiple cell wall motifs is required for *Lp*^{NC8} mediated larval growth promotion.

(a) *y,w* and *y,w,Dredd* larval longitudinal length after inoculation with 10^9 CFUs of *Lp*^{NC8} (n=55), Δ*dlt*$_{op}$ (n=50) and PBS (n=45), for the germ-free condition. Larvae were collected 5 days after association and measured as described in the methods section. Center values in the graph represent means and error bars represent SD. *ns* represents absence of statistically significant difference; ****: p<0,0001. Representative graph from one out of three independent experiments. (b) Number of *y,w* and *y,w,Dredd* emerged pupae scored over time for eggs associated with strains *Lp*^{NC8}, Δ*dlt*$_{op}$ and PBS for the germ-free condition. Forty

germ-free eggs of each genotype were associated independently with 10^9 CFUs of each one of the strains in 10 biological replicates. The number of pupae was scored every 24h. Representative graph from one out of three independent experiments. (c) Day when fifty percent of pupae emerge during a developmental experiment (D50) for *y,w* and *y,w,Dredd* GF eggs associated with strains Lp^{NC8}, Δdlt_{op} and PBS (for the GF condition). Center values in the graph represent means. *ns* represents absence of statistically significant difference; ****: p<0,0001. (d) Cell wall components of *L. plantarum* induce host intestinal transcriptional responses via a DAP type PG-responsive NF-κB-dependent signaling pathway (PGRP-LE/Imd/Relish cascade) and yet unknown signaling cascade(s), triggered by direct sensing of cell walls bearing D-alanylated TA. Other bacterial signals beyond PG and D-alanylated TA contribute to ensure *Drosophila* optimal growth. For exact *p* values see Supplementary Table 4.

Europe PMC Funders Author Manuscripts

Europe PMC Funders Author Manuscripts

Table 1

Loci of the insertions selected in the screen.

Mutant number	Locus of pVI110 disruption	Annotation
1-74	*lp_0594*	Malate transport protein (*mlep1*)
6-20	*lp_2021*	Serine-type D-ala-D-ala carboxypeptidase (*pbpX2*)
14-9	*IG lp0616-lp0617*	Intergenic region between *secE* and *nusG*
14-10	*lp_3240*	PTS system, beta-glucosides-specific EIIABC component (*pts28ABC*)
17-57	*lp_2466*	Prophage P2b protein 15, terminase large subunit
18-65	*lp_1944*	Multidrug ABC transporter
22-19	*lp_2027*	Chaperone, heat shock protein DnaK